Video-based analysis of head-torso coupling during lateral impacts under passive and co-contracted conditions

Pawel Kudzia[1,4], Gabrielle R. Booth[1,2,4], Kristen Reynier[3], Matthew Panzer[3], and Peter A. Cripton[1,4]

[1]School of Biomedical Engineering, University of British Columbia, Vancouver, BC, Canada
[2]MEA Forensic Engineers & Scientists, 23281 Vista Grande Drive, Laguna Hills, CA, USA
[3]Center for Applied Biomechanics, University of Virginia, Charlottesville, VA, USA
[4]Orthopedic and Injury Biomechanics Group, Departments of Mechanical Engineering and Orthopedics and ICORD, Blusson Spinal Cord Centre, Vancouver, BC, Canada

Keywords: Head-torso coupling·Kinematic response·Video-based motion analysis·Muscle activation

Corresponding authors:

Pawel Kudzia
School of Biomedical Engineering
University of British Columbia
6088 University Boulevard
Vancouver, BC, V6T 1Z3
Canada
pawel.kudzia5@gmail.com

Peter A. Cripton
School of Biomedical Engineering
University of British Columbia
6088 University Boulevard
Vancouver, BC, V6T 1Z3
Canada
pcripton@ubc.ca

Clinical trial number: not applicable.

Abstract word count: 235
Manuscript word count: 5,715
Figures: 6
Tables: 3

Abstract

Purpose Current surrogate necks and computational models lack empirical data on in vivo head-torso coupling across muscle activation states, limiting their biofidelity during impact testing. This study quantified head and torso kinematics and head-torso coupling during controlled lateral impacts under passive and co-contracted cervical muscle conditions.

Methods We conducted a secondary video analysis of high-speed footage (500 Hz) from Reynier et al. (2020), tracking frame-by-frame head and torso motion in 19 male participants during standardized lateral impacts (3.7 kg padded impactor at 2.0 m/s). Participants experienced impacts under passive (relaxed) and maximally co-contracted muscle conditions. Outcome measures included peak displacement, path length, head-torso relative excursion, velocity time lag, and peak linear kinematics.

Results Co-contraction reduced peak head displacement by 30% (14.2 ± 3.4 cm to 10.0 ± 3.6 cm, $p < 0.001$, $d = -1.51$) and path length by 21% ($p < 0.001$), with all 19 participants showing displacement reductions. Head-torso relative excursion decreased by 36% (11.3 ± 3.3 cm to 7.2 ± 3.2 cm, $p < 0.001$, $d = -1.35$), and velocity time lag shortened from 88 to 66 ms ($p = 0.002$). Peak linear acceleration remained unchanged (10.3 ± 0.9 g vs. 10.1 ± 1.0 g, $p = 0.415$), while peak head velocity decreased by 6% ($p = 0.003$). Peak angular velocity and angular acceleration also remained unchanged ($p = 0.320$ and $p = 0.820$).

Conclusion Cervical muscle co-contraction reduces head displacement by mechanically coupling the head to the torso, constraining displacement and velocity without altering peak acceleration or angular kinematics. These coupling metrics provide validation targets for surrogate neck designs and computational head-neck models incorporating active musculature.

Introduction

Inaccurate surrogate neck designs compromise our ability to predict and prevent traumatic brain injury. Sports-related concussions affect an estimated 1.4 to 3.8 million athletes annually in the United States [1, 2]. Reducing these injuries requires accurate laboratory testing with surrogates that replicate human biomechanics. Current anthropomorphic test devices (ATDs) and human body models (HBMs) lack empirical data on head-torso coupling needed to replicate human neck mechanics during impacts [3, 4]. This gap compromises safety testing across sports and automotive applications. This study addresses that gap through simultaneous measurement of both segments.

Peak acceleration provides an incomplete picture of the kinematic environment that causes brain injury. Brain tissue strain depends on spatial displacement and rotational velocity throughout the impact, not instantaneous acceleration maxima [5, 6]. Accelerometers measure motion at discrete anatomical locations but miss relative displacement between body segments [7–9]. Angular acceleration generates shear strains within brain tissue, causing diffuse axonal injury even without skull fracture [7, 8]. Spatial displacement and rotational kinematics predict concussion risk more accurately than peak linear acceleration alone [9].

Head-torso coupling determines head displacement during impact as much as impact severity itself. The torso anchors the system, and coupling strength dictates whether the head moves independently or as part of a larger linked mass. Researchers have measured head-to-torso kinematics during rear-end whiplash impacts and soccer heading, but these loading conditions differ from the direct lateral impacts common in contact sports [10, 11] and lateral automobile collisions. Quantifying coupling during lateral head impacts requires simultaneous measurement of both segments throughout the impact sequence.

Head-torso coupling modulates the head's kinematic response by changing its effective mass. When the head moves independently, impact forces accelerate only the isolated head mass (~4.5 kg). Active muscle co-contraction mechanically couples the head to the torso, engaging additional body mass and reducing

head kinematic response [12]. Video reconstruction of NFL helmet collisions demonstrated this principle: striking players who aligned head, neck, and torso before impact transferred momentum through the linked segment, while struck players whose heads moved independently experienced greater accelerations [12, 13]. Laboratory studies confirm that greater neck strength and anticipatory muscle activation reduce peak linear and angular velocity after impulsive loading [14, 15]. Coupling provides this protective effect by distributing impact energy across a larger effective mass rather than by reducing peak contact forces.

The degree of head-torso coupling may influence injury risk independently of peak acceleration, though computational models indicate this effect diminishes at higher severities where muscular forces become negligible [16, 17]. Despite this limitation, cervical muscle activation represents the most readily modifiable parameter influencing coupling at sub-catastrophic impact levels. Athletes achieve neuromuscular adaptations through training spanning weeks, whereas helmet designs or rule modifications require extended development [18, 19]. No previous study has directly measured head-torso coupling through simultaneous tracking of both segments in living humans.

Surrogate neck developers require empirical coupling data to address design limitations. The Hybrid III neck assembly, the current standard for automotive and sports equipment testing, demonstrates these design shortcomings. Its quasi-static bending stiffness exceeds that of a relaxed human neck by a factor of three yet represents only one-third the stiffness of a tensed neck [20]. Its developers validated it only for sagittal plane motion, and it performs poorly in lateral bending [21, 22]. No existing surrogate modulates mechanical properties based on muscle activation state. Researchers adopt a single intermediate stiffness that represents neither the passive nor the actively braced human neck [3]. Validating new biofidelic designs requires *in vivo* data showing how segment coupling changes across muscle activation conditions [23, 24].

Quantifying head-torso coupling requires simultaneous tracking of both segments in a common reference frame. Accelerometers require double integration to obtain position, introducing drift errors. Video tracking

with fiducial markers measures positions directly, achieving average errors of 1-1.5 mm during football head impacts [25]. Integrated position signals outperformed peak acceleration for characterizing impact kinematics in football players [26]. Direct position measurement avoids error accumulation while providing spatial trajectory information. High-speed video systems can track multiple markers simultaneously, enabling reconstruction of body segment motion throughout impact sequences [27].

We conducted a secondary video analysis to simultaneously measure head and torso kinematics during controlled lateral head impacts. We processed high-speed footage from Reynier et al. (2020) to track both segments in 19 participants during non-injurious impacts (3.7 kg padded impactor at 2 m/s) under passive and co-contracted conditions. We reconstructed segment trajectories and quantified head-torso coupling throughout the impact sequence. We hypothesized that cervical co-contraction reduces head displacement relative to the torso by increasing mechanical coupling between segments. These data provide the *in vivo* validation targets needed to develop more biofidelic surrogate necks and human body models.

.

Materials and Methods

Study design

We quantified head-torso coupling by analyzing high-speed video footage from controlled human head impact experiments. We conducted a secondary analysis of video recordings from Reynier et al. (2020), who delivered standardized lateral impacts to human volunteers under passive and co-contracted muscle conditions. Our analysis extracted frame-by-frame positional data for both head and torso segments throughout each impact, extending beyond Reynier's original focus on head-only kinematics measured via instrumented mouthpieces. We tracked complete movement trajectories to quantify how muscle activation alters the mechanical coupling between head and torso during non-injurious impacts.

Participants

The original study enrolled 20 healthy male volunteers. The mean participant age was 22.8 ± 3.0 years, height was 177.4 ± 3.5 cm, and body mass was 78.2 ± 9.5 kg. Reynier et al. excluded individuals with any history of concussion, neurological conditions, or recent musculoskeletal injuries. All participants provided written informed consent for both the original data collection and future secondary analyses. The University of Virginia Institutional Review Board for Health Sciences Research approved the original experimental protocol (IRB-HSR #20486, "Non-Injurious Head Motion in Human Subjects," Principal Investigator: M.B. Panzer). We obtained and used video recordings for 19 of the original 20 participants for this secondary analysis.

Experimental impact protocol

A pendulum system delivered standardized lateral impacts to each participant's head. The pendulum consisted of a 3.7 kg padded impactor covered with 6.35 mm polyurethane foam, suspended by two wires to ensure consistent impact trajectory [28]. This design delivered impacts at a standardized location 75 mm above the right tragus at 2.0 m/s velocity (Figure 1). A burned restraining filament released the pendulum for each trial, ensuring precise timing control. Participants wore an additional 19.05 mm foam pad secured by a swimming cap to standardize impact conditions and protect against injury (Reynier et al. 2020).

We tested two distinct muscle activation conditions to evaluate cervical muscle engagement effects on impact response. The passive condition delivered impacts within a randomized 20-second window without any countdown or warning, preventing anticipatory muscle activation. Surface electromyography confirmed minimal sternocleidomastoid activation during the passive condition. The co-contracted condition provided participants with a 3-second countdown before impact, during which they maximally contracted their bilateral neck muscles following standardized instructions. All participants completed the passive condition trials first to preserve the element of surprise and prevent learned anticipatory responses.

The original experimental protocol collected three synchronized data streams during each impact. Instrumented mouthpieces containing six-degree-of-freedom sensors (6DX Pro; DTS) measured head accelerations at 10,000 Hz. Surface electromyography (EMG) electrodes recorded bilateral sternocleidomastoid and upper trapezius muscle activity at 2,000 Hz. High-speed video cameras (MEMRECAM GX1, NAC Image Technology) captured the complete impact sequence at 500 Hz. Our analysis focused exclusively on the video footage to extract both head and torso position trajectories that previous accelerometer-based analyses could not capture.

<<<<<<<<<<<<<<<<<<Figure 1>>>>>>>>>>>>>>>>>>

Video processing and motion tracking

We calibrated high-speed video recordings to measure head and torso kinematics during all impact trials. We processed two recordings from each participant capturing both passive and co-contracted conditions, with each video including at least 50 milliseconds before impact and 500 milliseconds after impact. This duration ensured complete capture of pre-impact positioning, impact response, and recovery phases. We established the scale through known reference distances visible in each recording. The pendulum apparatus dimensions, standardized laboratory equipment, and calibration markers provided multiple reference measurements throughout the recording volume. We verified calibration accuracy by measuring at least five known distances in different orientations and cross-validating against documented apparatus specifications, achieving measurement accuracy within ±2% across the entire field of view.

We tracked a point on the head and a point on the torso frame-by-frame to quantify two-dimensional motion throughout each impact sequence. Using Tracker software (Open-Source Physics, version 6.2.0), we digitized distinct anatomical points (500 Hz). A high-contrast marker dot on each participant's protective cap provided a consistent head tracking point across all trials. We visually identified torso tracking points in the upper cervicothoracic region for each participant, selecting visible features such as clothing

landmarks (buttons, seams) or anatomical references (supraclavicular notch, upper trapezius contour). The absence of a standardized torso marker meant that tracking point locations varied between participants. During digitization, the operator qualitatively evaluated each trial for marker motion relative to the underlying anatomy and observed minimal marker-tissue artifacts across all trials. All 38 trials (19 participants × 2 conditions) met quality standards for marker visibility and landmark identification. We tracked both head and torso points in the medial-lateral (Y-axis, impact direction) and superior-inferior (Z-axis) planes throughout each sequence. A single trained operator digitized all trials to maintain consistency. Because each participant served as their own control, any systematic digitization bias affected both conditions equally and cannot explain the within-subject differences we report.

Signal processing and kinematic calculations

We processed position data through a standardized filtering and synchronization pipeline before calculating kinematic variables. We applied a fourth-order Butterworth low-pass filter with 50 Hz cutoff frequency using zero-phase filtering, selected to preserve the primary kinematic content while attenuating digitization noise. We derived velocity and acceleration using central differences for interior points and single-sided differences at endpoints. We smoothed the resultant acceleration time series with a 3-point moving average to reduce high-frequency noise amplified by double differentiation. We synchronized all trials to movement onset ($t = 0$), defined as head resultant velocity first exceeding 30 cm/s. This threshold exceeded baseline noise (5.0 ± 1.0 cm/s) by six standard deviations, ensuring reliable onset detection. We extracted data from -50 ms to 500 ms relative to movement onset.

We calculated kinematic variables to quantify instantaneous motion, cumulative displacement, and head-torso coupling (see Table 1 for details). Linear kinematics include peak resultant velocity and acceleration. We calculated head angular velocity using the torso position at movement onset as the pivot point, representing head rotation about the base of the neck. We calculated angular acceleration as the time derivative of angular velocity and applied a fourth-order Butterworth filter at 50 Hz to both angular

quantities. We calculated peak displacement as maximum straight-line distance from initial position, and displacement at 100 ms and 200 ms post-onset. We calculated total path length as cumulative Euclidean distance over the first 500 ms post-impact. For coupling metrics, we calculated head-torso relative excursion as the change in distance between the two tracking points from onset. We calculated the time lag as the difference in timing between head and torso peak values for each metric. We provide complete definitions and formulas for all variables in Table 1. Because our torso tracking points varied slightly between participants, we checked whether using a fixed versus moving torso pivot affected angular velocity calculations. The difference was negligible (<0.1% at peak) because peak angular velocity occurs within the first 20 ms of impact, when torso displacement remains small (<0.5 cm).

<<<<<<<<<<<<<<<<<<**Table 1**>>>>>>>>>>>>>>>>>>

Statistical analysis

We calculated percent change as ((co-contracted − passive) / |passive|) × 100%. We calculated Cohen's d effect sizes as the mean difference divided by the pooled standard deviation, interpreting values as small (|d| = 0.20–0.49), medium (|d| = 0.50–0.79), or large (|d| ≥ 0.80). We examined individual response consistency using linear regression of passive versus co-contracted displacement values. We report coefficients of determination (R^2) to characterize relationships between conditions. We did not apply corrections for multiple comparisons because we prioritized effect size interpretation over strict null-hypothesis significance testing, and our primary conclusions rest on large effect sizes (d > 1.0) rather than marginal p-values.

We generated mean waveforms by interpolating all individual trials to a common time vector, then calculating mean and standard deviation at each time point. The common time vector spanned from 50 ms before movement onset to 500 ms after, with 1 ms resolution (551 time points). We display individual participant peak values as boxplots showing medians, interquartile ranges, and full data ranges. We display

spatial trajectory patterns for four representative participants to illustrate the spatial information that video tracking provides; the Appendix contains complete trajectory data for all participants. We performed all analyses in MATLAB R2024b (MathWorks, Natick, MA) and report means ± standard deviations with 95% confidence intervals.

Results

Video-derived spatial trajectories

Co-contraction reduced head displacement in all 19 participants (Figure 2; Table 2). Head trajectories followed a consistent pattern, moving laterally and inferiorly from the initial position. Co-contraction constrained these trajectories closer to the starting position, reducing peak displacement by 30% ($p < 0.001$, $d = -1.51$). Individual reductions ranged from 6% to 62%. Head path length decreased by 21% ($p < 0.001$). Torso displacement showed a modest 10% reduction ($p = 0.026$), though individual responses varied widely, ranging from a 33% increase to a 36% decrease. Some participants' torsos displaced further under co-contraction, possibly reflecting whole-body stiffening that transmitted more pendulum energy to the torso. Torso path length remained unchanged.

Passive and co-contracted displacement values correlated across participants (Figure 3). All 19 participants fell below the equality line, confirming universal reduction with co-contraction. Both head and torso regressions yielded slopes of 0.70, indicating that participants with larger passive displacements showed proportionally larger reductions with co-contraction.

<<<<<<<<<<<<<<<<<<**Figure 2**>>>>>>>>>>>>>>>>>>

<<<<<<<<<<<<<<<<<<**Figure 3**>>>>>>>>>>>>>>>>>>

Head-torso coupling

Co-contraction reduced head excursion relative to the torso by 36-38% across all time points (Figure 4; Table 2). Peak relative excursion decreased from 11.3 ± 3.3 cm to 7.2 ± 3.2 cm ($p < 0.001$, $d = -1.35$), and participants reached this peak 76 ms earlier on average ($p = 0.004$). Individual reductions in peak relative excursion ranged from 2% to 72%.

Co-contraction also reduced the temporal lag between head and torso motion. The velocity time lag decreased in magnitude from −88 ± 20 ms to −66 ± 29 ms ($p = 0.002$, $d = 0.83$; Table 2), indicating more

synchronous segment motion. Time lag represents t(head peak) minus t(torso peak); negative values indicate the head peaked first. The acceleration and displacement time lags showed no significant changes (Table 2).

<<<<<<<<<<<<<<<<<<**Table 2**>>>>>>>>>>>>>>>>>>

<<<<<<<<<<<<<<<<<<**Figure 4**>>>>>>>>>>>>>>>>>>

Head and torso kinematics

Co-contraction altered head velocity but not head acceleration (Table 3, Figure 5). Peak head velocity decreased by 6% ($p = 0.003$, $d = -0.78$), while peak head acceleration remained unchanged ($p = 0.415$). Head velocity and acceleration peaked within the first 50 ms following impact, with waveforms returning toward baseline by 200 ms in both conditions.

Torso kinematics remained unchanged between conditions (Table 3, Figure 5). Peak torso velocity and acceleration showed no significant differences ($p = 0.865$ and $p = 0.713$, respectively). Torso peak values were smaller than head values, with peak velocity approximately one-third and peak acceleration approximately one-fifth of head magnitudes.

Angular kinematics

Head angular kinematics remained unchanged between conditions (Table 3, Figure 6). Peak angular velocity showed a non-significant 6% reduction ($p = 0.321$, $d = -0.23$), and peak angular acceleration showed a non-significant 1% reduction ($p = 0.821$, $d = -0.05$). Angular velocity and acceleration waveforms followed similar temporal patterns in both conditions, peaking within 50 ms of impact onset.

<<<<<<<<<<<<<<<<<<**Table 3**>>>>>>>>>>>>>>>>>>

<<<<<<<<<<<<<<<<<<**Figure 5**>>>>>>>>>>>>>>>>>>

Discussion

Cervical muscle co-contraction reduced head displacement by 30% and head-torso relative excursion by 36% while leaving peak linear acceleration unchanged. These findings indicate that bracing constrains head displacement and velocity rather than reducing peak acceleration. Video-based tracking of both segments enabled direct measurement of coupling dynamics throughout the impact sequence.

The results support the hypothesis that cervical muscle activation reduces head displacement through increased head-torso coupling. Co-contraction decreased both relative excursion and time lag between segments. Both head and torso displacement showed slopes of 0.70 relating passive to co-contracted values (Figure 3), indicating proportional constraint regardless of baseline displacement. This pattern suggests the head and torso moved as a more unified system. Finite element models support this mechanism, showing that active neck muscle force increases acceleration and velocity coupling between head and T1 through altered force transmission at the cervical spine [29]. NFL video reconstructions show similar effects, where players who braced before contact experienced reduced head displacement compared to unaware players [12, 13]. These trajectory changes matter for injury prediction because rotational kinematics and spatial displacement predict concussion risk more accurately than peak linear acceleration alone [30, 31]. The observed 6% reduction in peak head velocity reinforces the protective role of muscle activation beyond displacement constraint alone. Cervical bracing provides protection by constraining head trajectory and attenuating velocity, though these effects may diminish at higher impact severities where muscular forces become small relative to impact forces [16, 17].

The differential effects of co-contraction on displacement, velocity, and acceleration have implications for surrogate design. Current anthropomorphic test devices cannot capture the coupling changes we observed. The Hybrid III neck operates at a single intermediate stiffness representing neither the passive nor actively braced human neck. Both Hybrid III and Q-series ATDs produce reduced head rotation and neck excursions

compared to human volunteers due to rigid thoracic spine design [32]. Variable neck properties are technically feasible, as THOR-NT muscle cables significantly stiffen neck response by reducing occipital condyle joint laxity [22]. Cadaveric testing cannot provide these validation data because cadavers lack active muscle response. Our displacement, velocity, and coupling metrics define the response envelope that biofidelic surrogates must replicate.

Three factors limit the generalizability of our findings. First, we analyzed male participants experiencing lateral impacts at a single severity, preventing conclusions about sex differences, impact direction effects, and velocity-dependent responses. Second, manual video digitization captures position with lower temporal resolution (500 Hz) than direct sensor measurement (10,000 Hz). Our video-based surface tracking shares limitations with skin-mounted sensors that over-predict kinematics [27]. Torso tracking presented additional challenges because Reynier et al. (2020) did not record the original footage for motion tracking purposes. Variability in visible anatomical landmarks contributed to substantial inter-subject differences in torso measurements (CV = 56% for torso acceleration) [28]. This variability does not undermine our primary conclusions because head-torso relative excursion showed consistent large effect sizes (d = -1.35 to -1.67). The paired within-subject design ensures that digitization characteristics remain constant across conditions for each participant, isolating muscle activation effects from measurement variability.

These methodological differences caution against direct comparison with Reynier et al. (2020), who measured at the head center of mass using instrumented mouthguards. Despite these differences, both approaches found unchanged peak acceleration between muscle conditions, reinforcing this finding's robustness. Third, our protocol examined only two discrete muscle activation states, whereas athletes continuously adjust cervical posture and activation patterns before contact [15].

Future research should prioritize testing female participants to establish sex-specific coupling mechanics, given documented differences in neck strength and head-neck anthropometry [14, 19]. EMG-controlled

protocols can quantify graded muscle activation levels rather than discrete states. Examining multiple impact velocities and directions will establish how coupling effectiveness varies across the biomechanical range athletes experience. Cervical spine kinematics vary continuously during active movement, with alignment and stiffness changing dynamically with position and direction [33–35].

Advances in computer vision offer opportunities to improve tracking precision while reducing operator-dependent variability. Markerless pose estimation frameworks such as DeepLabCut and OpenPose now achieve near-expert labeling accuracy with minimal training data [36–38] and have transformed movement analysis in clinical gait assessment and sports performance [39]. Applying similar approaches to impact biomechanics could expand tracking to full-body kinematic chains and extract data from existing video archives.

In conclusion, anticipatory muscle activation reduced head displacement through increased head-torso coupling in our sample of healthy male participants. Co-contraction constrained displacement, reduced relative excursion, and attenuated peak head velocity while leaving peak acceleration unchanged. Unanticipated impacts with relaxed musculature may place athletes at greater risk by allowing larger head excursions during contact. These coupling data provide empirical targets for developing anthropomorphic test devices and validating computational models with active cervical musculature. Replication with female participants and across higher severities remains an important next step.

Ethics approval. The original experimental protocol was approved by the University of Virginia Institutional Review Board for Health Sciences Research (IRB-HSR #20486, approved March 20, 2018). The present study is a secondary analysis of video recordings collected under that approved protocol.

Consent to participate. All participants provided written informed consent (approved March 12, 2018) for both the original data collection and future secondary analyses. The consent process included viewing a video demonstrating the head impact procedure prior to enrollment.

Consent for publication. Participants consented to use of video recordings for research purposes. Raw footage is not published due to participant identifiability. All published figures use de-identified trajectory data or images of an anthropomorphic test dummy.

Acknowledgements We thank all participants who volunteered for the original study. We also thank the Center for Applied Biomechanics at the University of Virginia for providing access to the high-speed video footage from Reynier et al. (2020).

Author Contributions. P.K.: Conceptualization, Methodology, Formal analysis, Investigation, Data curation, Visualization, Writing -- original draft, Writing -- review & editing. G.B.: Conceptualization, Video Analysis, Investigation, Data curation, Formal analysis, Writing -- review & editing. K.R.: Resources, Writing -- review & editing, Supervision (original data collection). M.P.: Resources, Writing -- review & editing, Supervision, Funding acquisition (original study). P.C.: Conceptualization, Methodology, Writing -- review & editing, Supervision, Project administration, Funding acquisition.

Competing interests. The authors declare no competing or financial interests.

Funding. This secondary analysis received support from the Natural Sciences and Engineering Research Council of Canada (NSERC). The original experimental data collection reported in Reynier et al. (2020) was supported by Football Research, Inc.

Data availability. Analysis code and processed kinematic summary data are publicly available at https://github.com/pkudzia/Paper---Head-torso-coupling. Individual participant position coordinates, velocities, accelerations, and displacement time series are available from the corresponding author upon reasonable request. Raw video footage requires approval from the University of Virginia IRB (IRB-HSR #20486) due to participant identifiability.

References

1. Gessel, L. M., S. K. Fields, C. L. Collins, R. W. Dick, and R. D. Comstock. Concussions among United States high school and collegiate athletes. *J. Athl. Train.* 42:495–503, 2007.
2. Kerr, Z. Y., S. W. Marshall, H. P. Harding Jr, and K. M. Guskiewicz. Nine-year risk of depression diagnosis increases with increasing self-reported concussions in retired professional football players. *Am. J. Sports Med.* 40:2206–2212, 2012.
3. Nelson, T. S., and P. A. Cripton. A new biofidelic sagittal plane surrogate neck for head-first impacts. *Traffic Inj. Prev.* 11:309–319, 2010.
4. Siegmund, G. P., K. M. Guskiewicz, S. W. Marshall, A. L. DeMarco, and S. J. Bonin. Laboratory validation of two wearable sensor systems for measuring head impact severity in football players. *Ann. Biomed. Eng.* 44:1257–1274, 2016.
5. Gabler, L. F., J. R. Crandall, and M. B. Panzer. Development of a metric for predicting brain strain responses using head kinematics. *Ann. Biomed. Eng.* 46:972–985, 2018.
6. Alshareef, A., J. S. Giudice, J. Forman, R. S. Salzar, and M. B. Panzer. A novel method for quantifying human in situ whole brain deformation under rotational loading using sonomicrometry. *J. Neurotrauma* 35:780–789, 2018.
7. Gennarelli, T. A., L. E. Thibault, J. H. Adams, D. I. Graham, C. J. Thompson, and R. P. Marcincin. Diffuse axonal injury and traumatic coma in the primate. *Ann. Neurol.* 12:564–574, 1982.
8. Zhang, L., K. H. Yang, and A. I. King. A proposed injury threshold for mild traumatic brain injury. *J. Biomech. Eng.* 126:226–236, 2004.
9. McIntosh, A. S., D. A. Patton, B. Fréchède, P.-A. Pierré, E. Ferry, and T. Barthels. The biomechanics of concussion in unhelmeted football players in Australia: a case-control study. *BMJ Open* 4:e005078, 2014.
10. Stemper, B. D., N. Yoganandan, and F. A. Pintar. Effect of head restraint backset on head-neck kinematics in whiplash. *Accid. Anal. Prev.* 38:317–323, 2006.
11. Caccese, J. B., T. A. Buckley, R. T. Tierney, K. B. Arbogast, W. C. Rose, J. J. Glutting, and T. W. Kaminski. Head and neck size and neck strength predict linear and rotational acceleration during purposeful soccer heading. *Sports Biomech.* 1–15, 2017.
12. Viano, D. C., I. R. Casson, and E. J. Pellman. Concussion in professional football: biomechanics of the struck player--part 14. *Neurosurgery* 61:313–27; discussion 327-8, 2007.
13. Pellman, E. J., D. C. Viano, A. M. Tucker, I. R. Casson, and J. F. Waeckerle. Concussion in professional football: reconstruction of game impacts and injuries. *Neurosurgery* 53:799–812; discussion 812-4, 2003.
14. Tierney, R. T., M. R. Sitler, C. B. Swanik, K. A. Swanik, M. Higgins, and J. Torg. Gender differences in head-neck segment dynamic stabilization during head acceleration. *Med. Sci. Sports Exerc.* 37:272–279, 2005.
15. Eckner, J. T., Y. K. Oh, M. S. Joshi, J. K. Richardson, and J. A. Ashton-Miller. Effect of neck muscle strength and anticipatory cervical muscle activation on the kinematic response of the head to impulsive loads. *Am. J. Sports Med.* 42:566–576, 2014.
16. Li, F., R. Lu, W. Hu, H. Li, S. Hu, J. Hu, H. Wang, and H. Xie. The influence of neck muscle activation on head and neck injuries of occupants in frontal impacts. *Appl. Bionics Biomech.* 2018:1–14, 2018.
17. Eckersley, C. P., R. W. Nightingale, J. F. Luck, and C. R. Bass. The role of cervical muscles in mitigating concussion. *J. Sci. Med. Sport* 22:667–671, 2019.
18. Collins, C. L., E. N. Fletcher, S. K. Fields, L. Kluchurosky, M. K. Rohrkemper, R. D. Comstock, and

R. C. Cantu. Neck strength: a protective factor reducing risk for concussion in high school sports. *J. Prim. Prev.* 35:309–319, 2014.
19. Schmidt, J. D., K. M. Guskiewicz, J. T. Blackburn, J. P. Mihalik, G. P. Siegmund, and S. W. Marshall. The influence of cervical muscle characteristics on head impact biomechanics in football. *Am. J. Sports Med.* 42:2056–2066, 2014.
20. Friedman, D., J. Paver, and R. Grzebieta. The development of IARVs for the Hybrid III neck modified for dynamic rollover testing. SAE Technical Paper. 2010.
21. Bartsch, A., E. Benzel, V. Miele, D. Morr, and V. Prakash. Hybrid III anthropomorphic test device (ATD) response to head impacts and potential implications for athletic headgear testing. *Accid. Anal. Prev.* 48:285–291, 2012.
22. Dibb, A., R. Nightingale, and V. Chancey. Comparative structural neck responses of the THOR-NT, Hybrid III, and human in combined tension-bending and pure bending. SAE Technical Paper. 2006.
23. Fonseca, G., P. Vakiel, and P. A. Cripton. UBC neck C4-C5: An anatomically and biomechanically accurate surrogate C4-C5 functional spinal unit. *Ann. Biomed. Eng.* 51:1802–1815, 2023.
24. Farmer, J., S. Mitchell, P. Sherratt, and Y. Miyazaki. A human surrogate neck for traumatic brain injury research. *Front. Bioeng. Biotechnol.* 10:854405, 2022.
25. Hernandez, F., L. C. Wu, M. C. Yip, K. Laksari, A. R. Hoffman, J. R. Lopez, G. A. Grant, S. Kleiven, and D. B. Camarillo. Six degree-of-freedom measurements of human mild traumatic brain injury. *Ann. Biomed. Eng.* 43:1918–1934, 2015.
26. Kuo, C., L. Wu, J. Loza, D. Senif, S. C. Anderson, and D. B. Camarillo. Comparison of video-based and sensor-based head impact exposure. *PLoS One* 13:e0199238, 2018.
27. Wu, L. C., V. Nangia, K. Bui, B. Hammoor, M. Kurt, F. Hernandez, C. Kuo, and D. B. Camarillo. In vivo evaluation of wearable head impact sensors. *Ann. Biomed. Eng.* 44:1234–1245, 2016.
28. Reynier, K. A., A. Alshareef, E. J. Sanchez, D. F. Shedd, S. R. Walton, N. K. Erdman, B. T. Newman, J. S. Giudice, M. J. Higgins, J. R. Funk, D. K. Broshek, T. J. Druzgal, J. E. Resch, and M. B. Panzer. The effect of muscle activation on head kinematics during non-injurious head impacts in human subjects. *Ann. Biomed. Eng.* 48:2751–2762, 2020.
29. Yan, Y., J. Huang, F. Li, and L. Hu. Investigation of the effect of neck muscle active force on whiplash injury of the cervical spine. *Appl. Bionics Biomech.* 2018:1–10, 2018.
30. Rowson, S., S. M. Duma, J. G. Beckwith, J. J. Chu, R. M. Greenwald, J. J. Crisco, P. G. Brolinson, A.-C. Duhaime, T. W. McAllister, and A. C. Maerlender. Rotational head kinematics in football impacts: an injury risk function for concussion. *Ann. Biomed. Eng.* 40:1–13, 2012.
31. Takhounts, E. G., M. J. Craig, K. Moorhouse, J. McFadden, and V. Hasija. Development of brain injury criteria (BrIC). *Stapp Car Crash J.* 57:243–266, 2013.
32. Seacrist, T., M. Samuels, J. F. García-España, K. B. Arbogast, E. A. Mathews, S. Balasubramanian, M. R. Maltese, D. Longhitano, and S. St Lawrence. Kinematic comparison of the Hybrid III and Q-series pediatric ATDs to pediatric volunteers in low-speed frontal crashes. *Ann. Adv. Automot. Med.* 56:285–298, 2012.
33. Bogduk, N., and S. Mercer. Biomechanics of the cervical spine. I: Normal kinematics. *Clin. Biomech. (Bristol, Avon)* 15:633–648, 2000.
34. Snodgrass, S. J., and H. R. Rhodes. Cervical spine posteroanterior stiffness differs with neck position. *J. Electromyogr. Kinesiol.* 22:829–834, 2012.
35. Liu, M., R. D. Quarrington, W. S. P. Robertson, B. Sandoz, and C. F. Jones. Passive neck stiffness and range of motion for males and females from early to late adulthood. *Spine J.* 26:633–641, 2025.
36. Mathis, A., P. Mamidanna, K. M. Cury, T. Abe, V. N. Murthy, M. W. Mathis, and M. Bethge. DeepLabCut: markerless pose estimation of user-defined body parts with deep learning. *Nat. Neurosci.* 21:1281–1289, 2018.
37. Nath, T., A. Mathis, A. C. Chen, A. Patel, M. Bethge, and M. W. Mathis. Using DeepLabCut for 3D markerless pose estimation across species and behaviors. *Nat. Protoc.* 14:2152–2176, 2019.

38. Stenum, J., C. Rossi, and R. T. Roemmich. Two-dimensional video-based analysis of human gait using pose estimation. *PLoS Comput. Biol.* 17:e1008935, 2021.
39. Stenum, J., K. M. Cherry-Allen, C. O. Pyles, R. D. Reetzke, M. F. Vignos, and R. T. Roemmich. Applications of Pose Estimation in Human Health and Performance across the Lifespan. *Sensors* 21:7315, 2021.

460 **Table 1.** Kinematic variable definitions and formulas. All variables derived from two-dimensional position
461 data in the frontal plane (Y = medial-lateral, impact direction; Z = superior-inferior), normalized to
462 movement onset. Categories include linear and angular kinematics, displacement metrics at peak and fixed
463 time points (100 ms and 200 ms post-onset), and coupling metrics describing head motion relative to torso.
464 For angular kinematics, y and z represent head position relative to torso position.

Variable	Units	Definition	Calculation Formula
Linear Kinematics			
Resultant Velocity	cm/s	Resultant linear velocity of head or torso, where vy and vz are velocity components in the medial-lateral and superior-inferior directions	$\sqrt{(vy^2 + vz^2)}$
Resultant Acceleration	g	Resultant linear acceleration of head or torso, where ay and az are acceleration components in the medial-lateral and superior-inferior directions and g is the acceleration due to gravity.	$\sqrt{(ay^2 + az^2)} / g$
Angular Kinematics			
Head Angular Velocity (ω)	rad/s	Angular velocity of head about torso, where y and z are head position relative to instantaneous torso position, and vy and vz are head velocity components	$(y \cdot vz - z \cdot vy) / (y^2 + z^2)$
Head Angular Acceleration (α)	rad/s²	Angular acceleration of head, computed as time derivative of angular velocity	$d\omega/dt$
Displacement Metrics			
Peak Displacement	cm	Maximum straight-line distance from initial position, where y_0 and z_0 are initial coordinates	$\sqrt{((y-y_0)^2 + (z-z_0)^2)}$
Displacement at Time t	cm	Displacement at specified time post-onset (e.g., 100 ms, 200 ms), where yt and zt are coordinates at time t	$\sqrt{((yt-y_0)^2 + (zt-z_0)^2)}$
Path Length	cm	Total distance traveled during first 500 ms post-impact, summed across consecutive frames	$\Sigma\sqrt{((yi+1-yi)^2 + (zi+1-zi)^2)}$
Coupling Metrics			
Head-Torso Relative Excursion	cm	Change in head position relative to torso from onset, where yrel(t) = yhead(t) - ytorso(t) and zrel(t) = zhead(t) - ztorso(t)	$\sqrt{((yrel(t) - yrel(0))^2 + (zrel(t) - zrel(0))^2)}$
Time Lag	ms	Temporal difference between head and torso peak values for a given metric	t(head peak) − t(torso peak)

465

466

Table 2. Displacement and coupling metrics for passive and co-contracted conditions (n = 19). Values are mean ± SD [95% CI]. Time lag = t(head peak) − t(torso peak); negative values indicate the head peaked first (acceleration, velocity), positive values indicate the head peaked after the torso (displacement). Δ% = percent change from passive to co-contracted. Paired t-tests; Cohen's d effect size.

Parameter	Passive	Co-contraction	Δ%	p	d
Head Path					
Peak Displacement (cm)	14.22 ± 3.44 [12.57, 15.88]	9.96 ± 3.57 [8.24, 11.68]	-30.0%	<0.001	−1.51
Time to Peak Displacement (ms)	271 ± 56 [244, 298]	220 ± 95 [174, 266]	-18.8%	0.004	−0.77
Displacement at 100ms (cm)	9.97 ± 1.36 [9.32, 10.63]	7.37 ± 1.20 [6.80, 7.95]	-26.1%	<0.001	-1.82
Displacement at 200ms (cm)	12.94 ± 2.39 [11.79, 14.09]	8.94 ± 2.58 [7.70, 10.19]	-30.9%	<0.001	-1.89
Path Length (cm)	19.07 ± 3.18 [17.53, 20.60]	15.02 ± 2.48 [13.83, 16.21]	-21.2%	<0.001	-1.66
Torso Path					
Peak Displacement (cm)	3.73 ± 0.99 [3.26, 4.21]	3.37 ± 0.90 [2.94, 3.81]	-9.7%	0.026	−0.56
Time to Peak Displacement (ms)	199 ± 42 [179, 219]	171 ± 49 [148, 195]	-13.9%	0.024	−0.57
Displacement at 100ms (cm)	1.89 ± 0.54 [1.63, 2.16]	2.36 ± 0.62 [2.06, 2.66]	24.7%	0.003	0.79
Displacement at 200ms (cm)	3.55 ± 0.88 [3.13, 3.98]	3.00 ± 1.02 [2.51, 3.49]	-15.5%	0.001	-0.89
Path Length (cm)	6.17 ± 1.43 [5.48, 6.86]	6.30 ± 1.36 [5.64, 6.95]	2.1%	0.611	0.12
Head excursion relative to the torso					
Peak (cm)	11.31 ± 3.32 [9.71, 12.91]	7.21 ± 3.15 [5.69, 8.72]	-36.3%	<0.001	-1.35
At 100 ms (cm)	8.22 ± 1.53 [7.48, 8.96]	5.13 ± 1.34 [4.48, 5.78]	-37.6%	<0.001	−1.66
At 200 ms (cm)	9.72 ± 2.30 [8.62, 10.83]	6.08 ± 2.14 [5.05, 7.11]	-37.5%	<0.001	−1.67
Time lag between head and torso peak values					
Displacement (ms)	71.9 ± 67.6 [39.3, 104.5]	48.6 ± 79.6 [10.3, 87.0]	-32.4%	0.096	-0.40
Velocity (ms)	-88.2 ± 19.9 [-97.8, -78.6]	-65.6 ± 28.9 [-79.5, -51.6]	-25.7%	0.002	0.83

Table 3. Peak kinematic parameters for head and torso (n = 19). Values are mean ± SD [95% CI]. Δ% = percent change from passive to co-contracted. Paired t-tests; Cohen's d effect size.

Parameter	Passive	Co-contraction	Δ%	p	d
Head					
Peak Velocity (cm/s)	149.7 ± 11.2 [144.3, 155.0]	140.0 ± 12.9 [133.8, 146.3]	-6.4%	0.003	−0.78
Peak Acceleration (g)	10.28 ± 0.87 [9.86, 10.70]	10.13 ± 1.04 [9.62, 10.63]	-1.5%	0.415	−0.19
Peak Angular Velocity (rad/s)	4.29 ± 0.98 [3.82, 4.77]	4.05 ± 0.90 [3.62, 4.49]	-5.6%	0.320	-0.23
Peak Angular Acceleration (rad/s²)	280 ± 67 [247, 312]	276 ± 64 [245, 307]	-1.3%	0.820	-0.05
Torso					
Peak Velocity (cm/s)	43.6 ± 11.0 [38.3, 48.9]	44.1 ± 12.5 [38.1, 50.2]	1.2%	0.865	0.04
Peak Acceleration (g)	2.29 ± 1.28 [1.67, 2.90]	2.19 ± 0.81 [1.80, 2.59]	-4.1%	0.713	−0.09

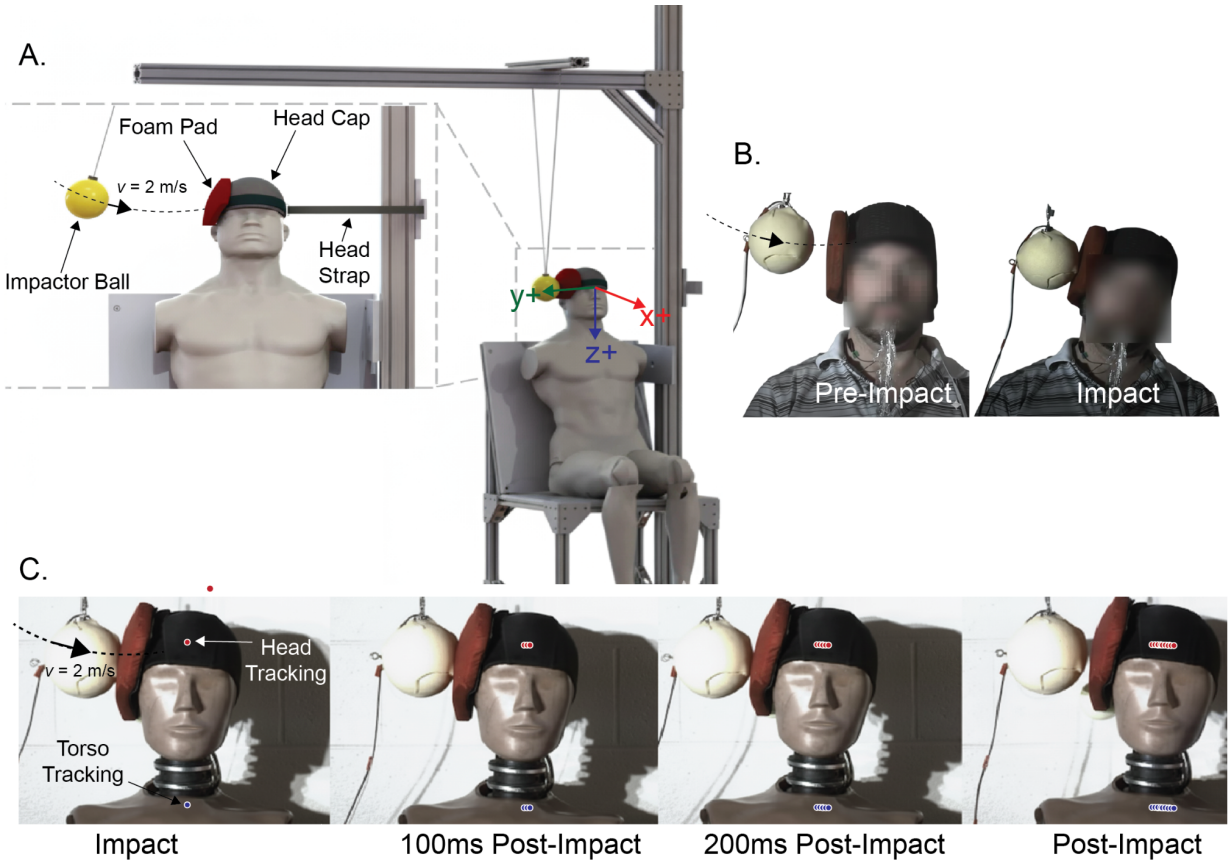

Figure 1. Experimental setup and video digitization method. (A) Bi-filament pendulum system delivering 2.0 m/s lateral impacts from a 3.7 kg padded impactor to a location 75 mm above the right tragus. High-speed cameras recorded at 500 Hz. (B) Representative impact sequence showing pre-impact positioning (left) and padded impactor contact (right). (C) Frame-by-frame digitization of head (red dot on protective cap) and torso (blue dot in upper cervicothoracic region) positions using Tracker software (Open-Source Physics, v6.2.0). An anthropomorphic test dummy demonstrates the digitization method for clarity.

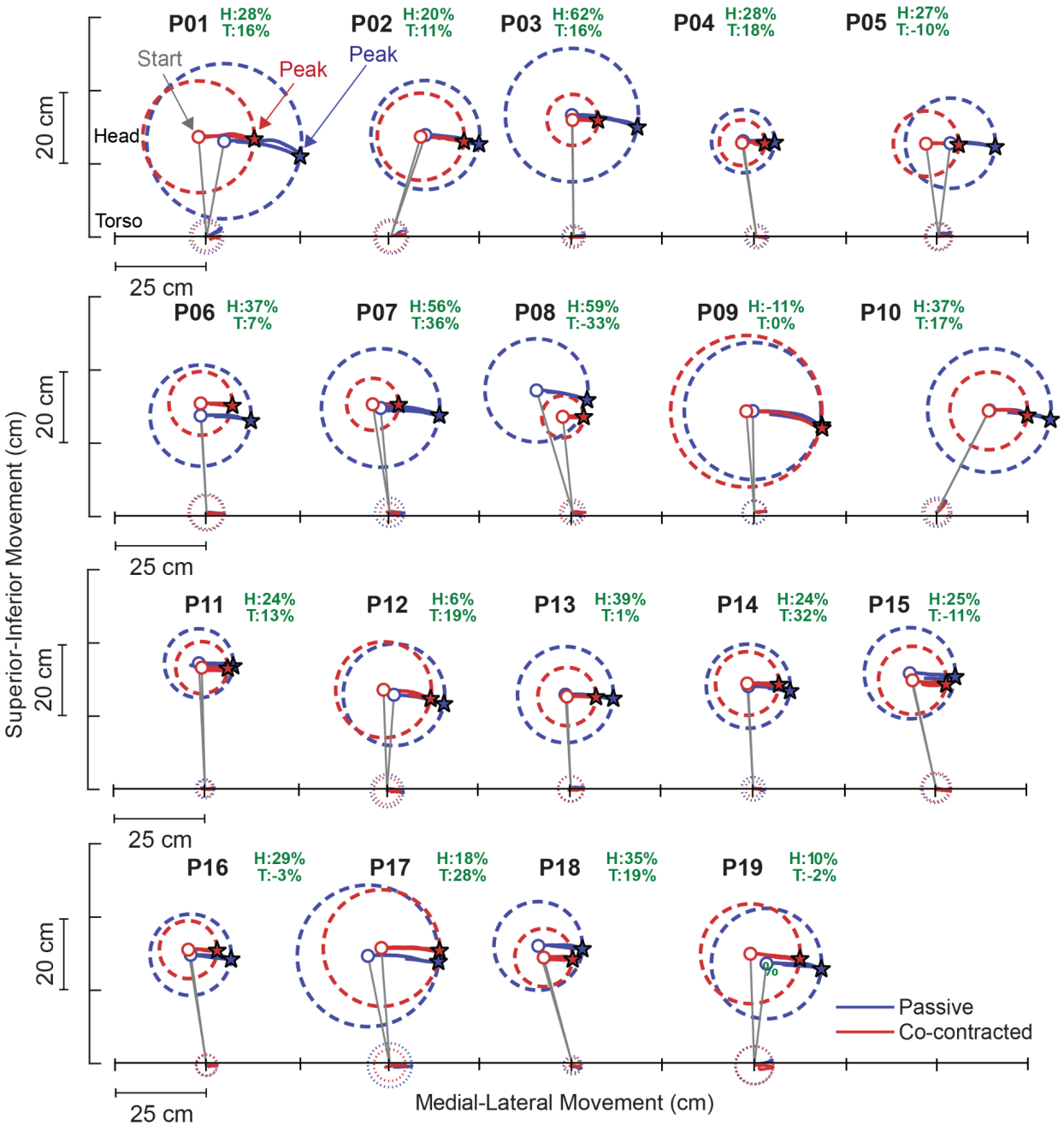

485

486 **Figure 2.** Individual head and torso trajectories during lateral impact (n = 19). Movement paths in the
487 medial-lateral and superior-inferior plane under passive (blue) and co-contracted (red) conditions, aligned
488 to torso starting position. Solid lines trace movement from initial position (circles) to peak displacement
489 (stars). Dashed circles indicate peak displacement magnitude. Green percentages show head (H) and torso
490 (T) displacement reductions with co-contraction; negative values indicate increased displacement. Gray
491 lines connect head and torso starting positions.

492

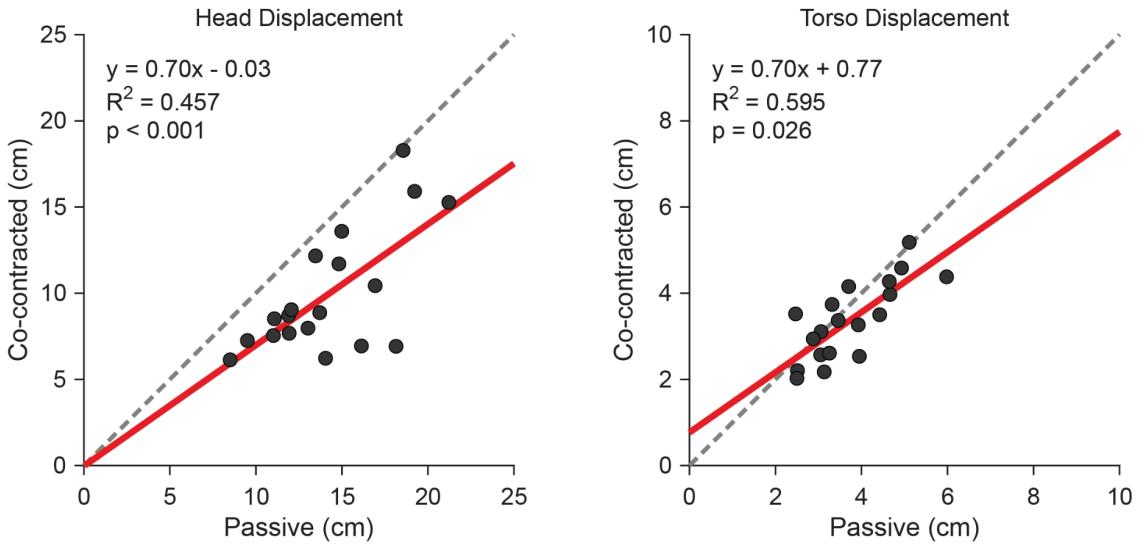

493

494 **Figure 3.** Individual participant displacement responses in passive versus co-contracted conditions (n =
495 19). Peak head displacement (left) and peak torso displacement (right). Gray dashed line indicates equality
496 between conditions; red line shows linear regression fit. Points below the equality line indicate reduced
497 displacement with co-contraction. Regression equations and R^2 values appear in each panel.

498

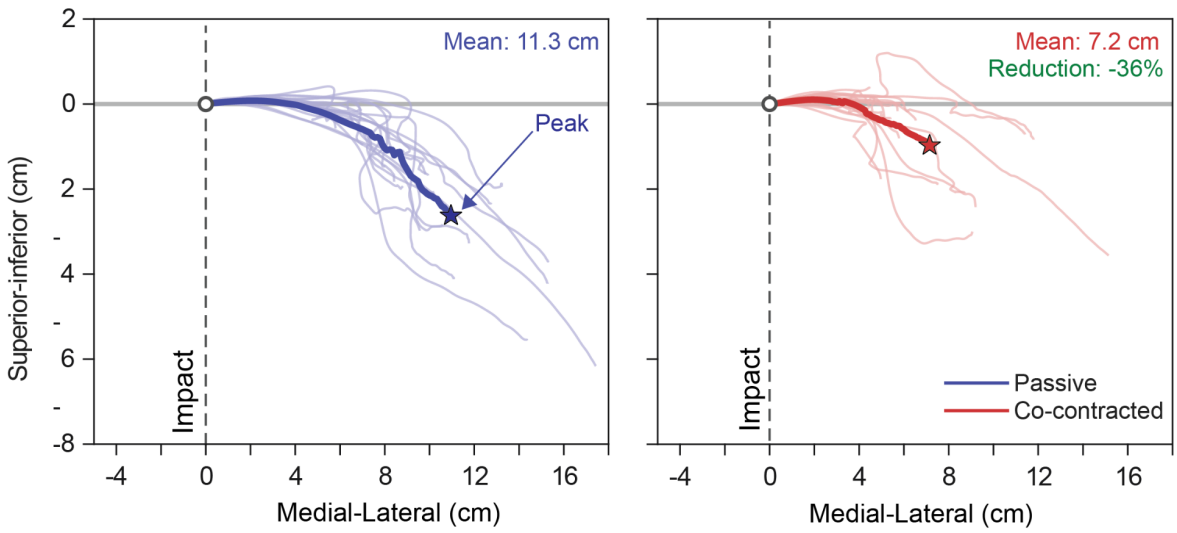

499

500 **Figure 4.** Head position relative to torso during lateral impact (n = 19). Movement paths in the medial-
501 lateral and superior-inferior plane, aligned to starting position (0, 0) and truncated at peak excursion.
502 Passive (left, blue) and co-contracted (right, red) conditions show individual trajectories (light lines) and
503 mean trajectory (dark line). Circles mark initial position; stars mark mean peak excursion.
504

505

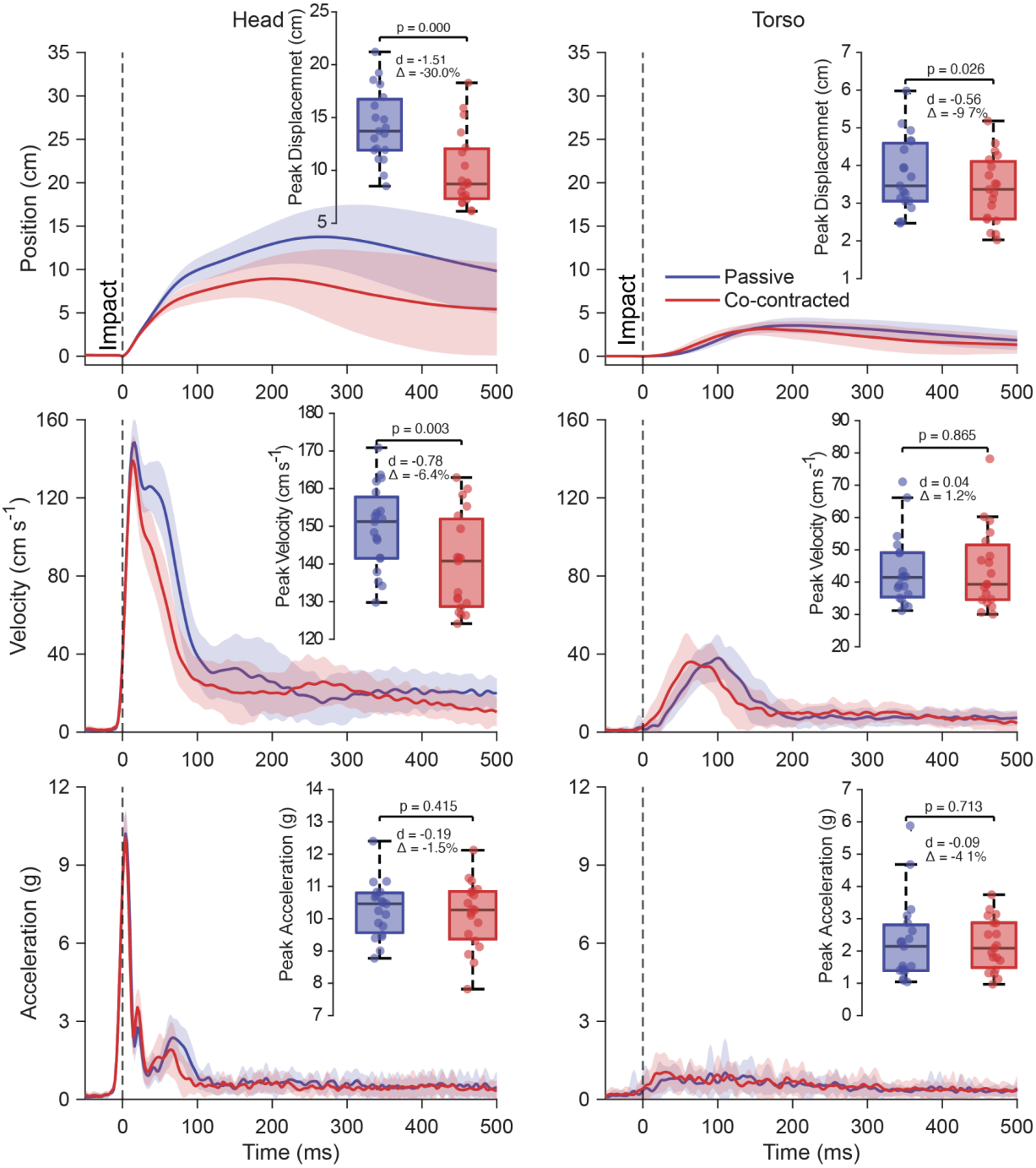

506

507 **Figure 5.** Head and torso kinematics during lateral impacts (n = 19). Position (top), velocity (middle), and
508 acceleration (bottom) for head (left) and torso (right) in passive (blue) and co-contracted (red) conditions.
509 Solid lines represent means; shaded regions represent ±1 SD. Dashed vertical line marks impact onset (t =
510 0 ms). Inset boxplots show peak values with individual data points, p-values, Cohen's d, and percent change.

511

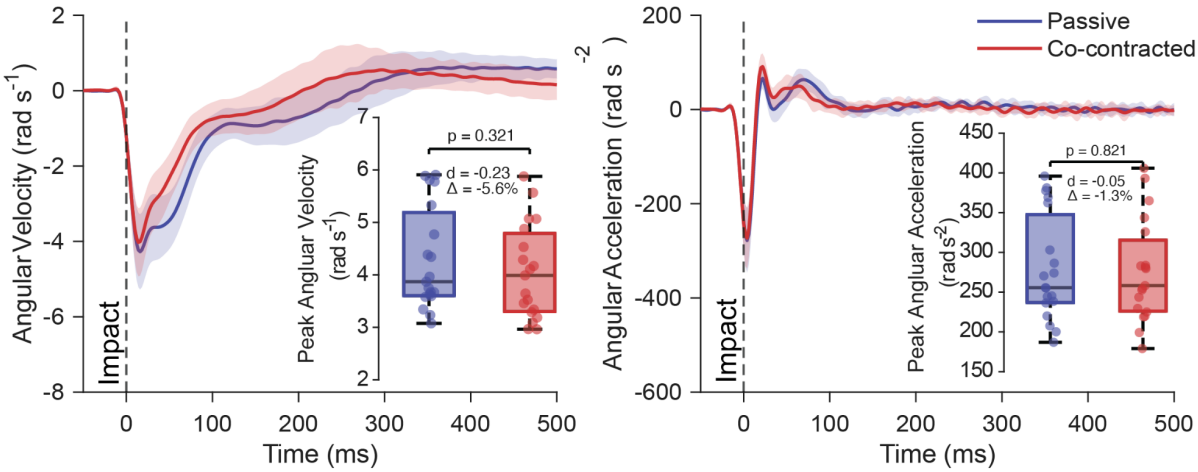

512

513 **Figure 6.** Head angular kinematics during lateral impacts (n = 19). Angular velocity (left) and angular
514 acceleration (right) in passive (blue) and co-contracted (red) conditions. Solid lines represent means;
515 shaded regions represent ±1 SD. Dashed vertical line marks impact onset (t = 0 ms). Inset boxplots show
516 peak values with individual data points, p-values, Cohen's d, and percent change.

517